Single foraminifera Mg/Ca analyses of past glacial-interglacial temperatures derived from G. ruber sensu stricto and sensu lato morphotypes

Anne Schmitt, Mary Elliot, K. Thirumalai, Carole La, Franck Bassinot, Jassin Petersen, Aurore Movellan, S.J. Jorry, J. Borgomano

Chemical Geology
April 2019, Volume 511, Pages 510-520
https://doi.org/10.1016/j.chemgeo.2018.11.007
https://archimer.ifremer.fr/doc/00472/58336/

Single foraminifera Mg/Ca analyses of past glacial-interglacial temperatures derived from *G. ruber* sensu stricto and sensu lato morphotypes

Schmitt A. [1, *], Elliot M. [1], Thirumalai K. [2], La C. [1], Bassinot F. [3], Petersen J. [1], Movellan A. [1, 4], Jorry Stephan [5], Borgomano J. [6]

[1] Laboratoire de Planétologie et Géodynamique UMR 6112, 44300 Nantes, France
[2] DEEPS, Brown University, 02912, RI, USA
[3] LSCE, 91191 Gif sur Yvette, France
[4] Ocean Zoom, 44300 Nantes, France
[5] IFREMER, 29280 Plouzané, France
[6] CEREGE-CNRS, 13545 Aix en Provence, France

* Corresponding author : A. Schmitt, email address : anais.schmitt@univ-nantes.fr

Abstract :

The ratio of magnesium to calcium (Mg/Ca) in foraminiferal shells is commonly used as a proxy for past ocean temperature. Recent advances in elemental analyses now enable single-specimen measurements of planktic foraminifera and thus, can provide information on past seasonal and interannual variability, owing to the near-monthly lifespan of foraminifera. In this study, we explore the temperature variance recorded by Mg/Ca in tests of foraminifera *Globigerinoides ruber*, a planktic species that occurs throughout the year in tropical waters. Using LA-ICP-MS, we characterize Mg/Ca variability in single specimens of two morphotypes of *G. ruber* picked from a sediment core retrieved offshore New Caledonia. We provide an estimate of the range of calcification temperatures for these morphotypes during five interglacial-glacial cycles over the last 1.55 Ma. First, we find significant and systematic differences between the morphotypes and second, the temperature difference between morphotypes does not remain constant through time. Our results highlight a progressive increase in surface-water temperatures during interglacials and a progressive decrease in glacial subsurface water temperatures. These changes in surface and subsurface temperatures potentially highlight a change in the stratification of the water column over the Mid-Pleistocene Transition. We conclude that single-specimen Mg/Ca on foraminiferal morphotypes can offer unique perspectives on paleoenvironmental reconstructions.

Keywords : *Globigerinoides ruber*, Mg/Ca ratio, Sea surface temperature, LA-ICPMS, Seasonality, Quaternary

1. Introduction:

The magnesium-to-calcium ratio (Mg/Ca) in foraminifera reflects the sea water temperature at the time of shell calcification (Eggins et al., 2003). Planktic foraminiferal Mg/Ca thermometry has emerged as a powerful tool in paleoceanography to reconstruct past ocean temperatures in the water column, and in particular, sea-surface temperatures (SST) (Barker et al., 2003; Dekens et al., 2002; Elderfield and Ganssen, 2000; Lea et al., 2000; Rosenthal et al., 2000). The standard approach is to measure ~20 to 30 monospecific specimens selected from each sample. These measurements are thought to reflect past temperature over the period of time represented by the sediment sample, commonly decades to millennia depending on regional accumulation rates and bioturbation mixing. Such reconstructions average out any inter-annual or seasonal temperature variability over the studied time interval (Anand et al., 2003; Barker et al., 2003).

Recently, several micro-analytical instrumentation techniques have been developed to characterize chemical element distributions within an individual foraminiferal shell (or test), including Laser Ablation ICP-MS (LA-ICP-MS) on planktic species (Billups and Spero, 1996; Eggins et al., 2004, 2003; Hathorne et al., 2003; Kısakürek et al., 2008; Leduc et al., 2009; Sadekov et al., 2009, 2008; Spero et al., 2015). Because foraminifera calcify over a period of weeks to a month (Spero et al. 1998), individual foraminiferal analyses (IFA) can yield insights into month-to-month and longer forms of temperature variability within the sampled time interval. Recent geochemical and statistical work has shown that in most locations, the IFA signal is dominated by seasonality i.e. the average peak-to-trough seasonal temperature variance during a sampled time interval (Sadekov et al., 2009; Thirumalai et al., 2013).

In this study, we focus on planktic foraminifera *Globigerinoides ruber* (white), a species widely used to reconstruct SST (Thirumalai et al., 2018, 2014). *G. ruber* has a broad

ecological gradient: it develops in oligotrophic waters ranging from 16 to 31°C and salinity from 22 to 49 PSU (Žarić et al., 2005). Its optimum temperature is ~26.5°C from (Bijma et al., 1990). This species is found between the surface and has been found as deep as 120 meters (Fairbanks et al., 1982; Kawahata et al., 2002; Kuroyanagi and Kawahata, 2004). Some studies have hypothesized specific habitat preferences for the two *G. ruber* morphotypes: *sensu stricto* (ss) and "Elongatus morphotypes"/*sensu lato* (sl) (Wang, 2000), whereas other studies have found no significant differences (Thirumalai et al., 2014). Assessing the effect of morphotypical variability on geochemical variability, and ultimately, its effect on temperature reconstructions is essential to generate accurate records of past climate.

Here, we focus on morphotypical variability in different morphotypes of *G. ruber* in downcore sediments taken offshore New Caledonia (23°S/163°E). Our study covers the Pleistocene period, which is marked by a shift in the dominant periodicity of glacial-interglacial cycles from 41 kyr obliquity cycles to higher amplitude 100 kyr eccentricity cycles, separated by the Mid Pleistocene Transition (MPT) circa ~800 ka. We reconstruct past seasonality using IFA of Mg/Ca of *G. ruber* (white). We measure a series of specimens from the same sample and estimate the maximum/minimum temperature variance at the New Caledonia margin. We first evaluate the reproducibility and the accuracy of core top temperature reconstructions and compare them with *in situ* temperature data (Behringer and Xue, 2004; Reynolds et al., 2002; Smith and Reynolds, 2004). Finally, we compare results over five climatic cycles during the last 1.5 Ma and test the statistical differences of temperature variance reconstructed from the two *G.ruber* planktic foraminifera morphotypes.

2. Material and Method:

2.1 Study area and modern hydrography

Samples of planktic foraminifera were selected from specific depths of deep-sea sediment core MD06-3018 (23°00'S, 166°09'E and 2470 m water depth) which is located on the eastern side of the New Caledonia Trough, ~60 km offshore of the island of New Caledonia (Figure 1). The age model of this sediment core has been derived from isotope stratigraphy and magnetic properties and spans the past 1.5 Ma (Russon, 2011).

At our site, World Ocean Atlas (WOA) 2005 SST values at 0 m depth, for the 1° by 1° grid range from winter (August) values of ~22 °C (Figure 1a) to summer (February) values of ~28 °C (Figure 1b), thus a maximum seasonal SST amplitude range of ~6°C. Surface waters are influenced by the South Equatorial Current (SEC) which transports warm waters from the western equatorial Pacific southwards (Bostock et al., 2006; Ridgway and Dunn, 2003) (Figure 1).

Precipitation over New Caledonia ranges from ~50 mm/month during the late winter and early spring to >140 mm/month in the summer rainy season. The mean-annual sea-surface salinity in the central New Caledonia Trough is 35.3 PSU with seasonal fluctuations driven by precipitation changes on the order of ~1.2 PSU (Delcroix and Lenormand, 1997).

Figure 1: Modern hydrodynamic surface water in New Caledonia. Present-day seasonal climatology in the New Caledonia core location (NOAA, WOA05): surface temperature (0m) during a. austral winter (August) b. austral summer (February) with Schematic surface water circulation regimes in the subtropical southwest Pacific. Abbreviations are as follows: SEC = South Equatorial Current, EAC = East Australian Current, SCJ = South Caledonian Jet.

Regarding the subsurface temperatures of this location we use Global Ocean Assimilation System potential temperature values from NOAA (2° spatial grid) recorded since 1854 (Smith and Reynolds, 2004) (Figure 2). The mixed layer depth at our site is estimated to be ~40 m in austral summer and ~130 m in austral winter, on average.

Figure 2: Potential Temperature profile and Salinity profile (0-200m), mean of the last 37 years, at the core location per month and depth (dotted black line) from NOAA, (GOAS). Red points correspond to the mean mixed layer depth during austral summer (40m) and austral winter (130m).

We compare mean monthly SSTs from global data with a daily resolved dataset from Uitoé close to Amédée lighthouse in New Caledonia (65 km to the core location). The daily sea surface temperature record provides more accurate representations of seasonal temperature variability with a larger variability of temperatures around 8 °C which is 2°C more than the maximum range estimated from monthly mean SST data sets. SST at Amédée are approximately 1 °C warmer and 1 °C colder than the mean monthly SST data. This comparison of local *in situ* versus 1°-1° SST's derived from global databases highlights larger-scale variability (Varillon et al., 2018) (Figure 3).

Figure 3: Daily and monthly sea surface temperature data at 5m depth since 1992 to 2001 from Uitoé.

2.2 Sample selection

The age model for marine core MD06-3018 yields a mean sedimentation rate of 3 cm/kyr and an age of 1550 ka at the base of the core-bottom. The core top (0-1 cm) is of Holocene age and was dated at 3660 years BP by radiocarbon (Russon et al., 2010). Russon et al, (2010) generated an SST record for the western New Caledonia margin using Mg/Ca measurement by ICP-AES of planktic foraminifera *G. ruber* (white) on this same sediment core. Results from this previous study showed that, for the last 1.55 Ma, mean interglacial periods temperatures were around 27 °C and mean glacial periods temperatures around 23 °C (Figure 4).

Figure 4: Oxygen Isotope (black) and Sea Surface Temperature (SST) (bleu) derived from Mg/Ca measurement on planktic foraminifera G. ruber white ss core MD06-3018 (adapted from Russon et al 2010). Marin Stage Isotopes (MIS) interpretation and samples selection position (red points) in both curves overs last 1.6 Ma. The Mid Pleistocene Transition (MPT) interval, is shown by background shading using the boundary dates of Head and Gibbard (2008).

We selected specific time intervals in sediment core MD06-3018 corresponding to 1cm thick sediment layers, which approximately span 300 years of deposition. Ten horizons were chosen corresponding to five interglacial/glacial periods over the past 1.55 Ma. Our strategy was to sample glacial-interglacial periods prior, during and after the Mid Pleistocene Transition (MPT). We selected samples from MIS 37/38 (40 kyr world), MIS31/32 and 15/16 (during the MPT) and finally MIS11/12 and MIS1 (Holocene)/2 (LGM) (100 kyr world) (Table 1).

Table 1 : Samples selection and LA-ICP-MS in single foraminifera measurement strategy, core MD06-3018. Corresponding marine isotope stage (MIS), depth of samples from which foraminifera were picked, corresponding age in ka, Glacial (G) or Interglacial period (IG), number of foraminifera G. ruber ss and G. ruber sl analysed per level, number of chambers and number of measurements per chamber analysed and finally the total number of ablations per level.

2.3 Analyses strategy

Within each wet-sieved sample, thirty individual foraminifera (15 *G. ruber* ss and 15 *G. ruber* sl) were picked from the 250-315 μm size fraction. The size fraction analysed was chosen to include only adult stages of this species and corresponds to the same size range used for Mg/Ca by ICP-AES measurements (Russon et al., 2010). For each individual, we chose to systematically measure the same two chambers (F-1, F-2). Each chamber was measured three times to obtain a reliable average for each shell (Figure 5). We refrained from measuring the final chamber after initial tests showed aberrant Mg/Ca values, potentially due to the presence of organic matter.

Prior to measurement, we intensively cleaned our foraminiferal samples. We performed the clay-removal step of Mg/Ca cleaning procedure described in (Barker et al., 2003) which was slightly modified as in Koho et al. (2017) and Petersen et al. (2017). We utilized the intensity-ratio calibration method for our measurement, detailed in de Villiers et al. (2002). First, the specimens were rinsed three times with 200 μL of ultra-pure water. Next, we used a 200 μL methanol rinse (twice) and followed that with three final rinses in ultra-pure water. Each time the samples were gently agitated with a vortex machine for 5 seconds and the liquid was removed with a Pasteur pipette. Such a procedure ensures that foraminiferal shells are not broken.

Figure 5: G. ruber white sensu stricto (ss) and sensu lato (sl) foraminifera defined by Wang et al, (2000) terminology, SEM picture from the core MD06-3018, after laser ablation measurement.
Location of the different holes measured in the two chambers (F-1; F-2) of the foraminifera.

2.4 LA-ICPMS operating conditions and instrument calibration

Our samples were analysed using a Laser Ablation (ArF excimer laser, 193 nm, Analyte G2, Photon machine Inc.) and Quadrupole Inductively Coupled Plasma Mass Spectrometry (820-MS varian) (LA-Q-ICP-MS) at the LPG, Nantes University (France). This tool is a direct sampling analytical technology that enables highly sensitive elemental analyses on solid samples. Laser sampling was conducted in a He atmosphere to maximize sample yield. A number of isotopes (^{24}Mg, ^{25}Mg, ^{26}Mg, ^{27}Al, ^{43}Ca, ^{44}Ca, ^{48}Ca, ^{47}Ti, ^{48}Ti, ^{55}Mn, ^{57}Fe, ^{88}Sr, ^{137}Ba, ^{208}Pb) were measured using a rapid peak hopping procedure as laser ablation proceeds through test walls.

Before every analytical session, the ICP-MS was tuned with the NIST SRM 612 reference material to minimise oxide formation ($ThO^+/Th^+ < 0.5$ %) and elemental fractionation ($^{238}U/^{232}Th$ close to 1) as well as to optimise the signal. All ICP-MS parameters are summarized in Table 2.

A typical laser ablation profile corresponds to ~30 seconds data acquisition of the background signal, followed by ablation of the chamber wall (duration approx. 30 s). The ablation process is stopped manually after visual inspection of the complete ablation of the chamber wall. Finally, another interval of background signal is measured (Figure 6). NIST 610 as well as an in–house carbonate standard obtained from the Royal Nertherland Institute for the Sea Research (NFHS) were ablated with a laser energy density of ~0.91 J/cm^2, between every five foraminifera analyses. The results for the NFHS carbonate standard are used for quality control and reproducibility.

Table 2: Summarized LA-ICP-MS operating conditions for technic.

2.5 Data processing

Mg/Ca ratios were calculated by normalization to the known trace element concentrations in the drift-corrected, bracketed analyses of the NIST 610 standard (Mg = 432 µg/g, Ca = 81.830 µg/g, relative standard deviation about 0.1 to 0.5 %, (Jochum et al., 2011)). Calibration of element/calcium ratios in calcium carbonate samples using a NIST glass standard has been demonstrated to be accurate for many elements when using a 193 nm laser (Hathorne et al., 2008). We use ^{43}Ca as our internal standard. We obtain the integrated average Mg/Ca ratio after excluding an initial elemental spike (Figure 6), that could reflect surface contamination or excess material ablated from the shell surface (identified on profiles using Glitter software). Finally, we convert Mg/Ca values into temperatures using the equation derived from 42 core top studies (24 core tops in the tropical and subtropical Atlantic and 18 core tops in the tropical Pacific), specific to the *G. ruber* white 250-350 µm (Dekens et al., 2002). This Mg/Ca calibration uses core depth as a metric for dissolution correction. The same equation is used for the two morphotypes of *G. ruber* :

$$Mg/Ca = 0.38 \exp 0.09 (SST - 0.61 (\text{core depth km}) - 1.6°C)$$

Figure 6: Typical G. ruber trace elements (Mg, Ca, Mn, Fe, Al and Ba) raw profiles in counts from laser ablation across one hole in one chamber. All tests have been ablated (profiled) from the outer to the inner surface (left to right).

2.6 Reproducibility and analytical precision:

We used two standards: the NIST 610 for a silicate glass matrix and the NFHS a carbonate matrix, measured several times a day and at each session to ensure adequate reproducibility. The relative standard error of the Mg^{24}/Ca^{43} ratio in NIST 610 for all sessions on this study was found to be ~2 % (0.06 mmol/mol), with a difference of 0.11 mmol/mol compared to the reference from Jochum (2011). Daily variations in the analysis of the standard NIST 610 is low (0.5 %), indicating appropriate analytical conditions for measurement. The carbonate standard is less homogeneous, where NFHS was used to evaluate the external reproducibility. During each analytical session, 7 to 9 NFHS standards were measured, and the relative standard error was found to be ~4 %. The largest Mg/Ca variability observed during one ablation profile for the NIST 610 was ~10 % relative standard deviation.

In order to quantify the reproducibility of the analytical method, related to natural variability within one sample, 3 replicates were analysed from the same sediment core level. In total, we analysed 86 foraminifera (MIS1 a, b, c), where we chose to replicate core-top sample (0-1 cm). The replicates of 30 foraminifera (15 *G. ruber* ss / 15 *G. ruber* sl) are named a, b, c (Figure 7; Table 1).

Figure 7: Reproducibility of the Holocene period with 3 replicates (a,b,c). Interquartile range of sea surface temperature (SST) derived from Mg/Ca in single foraminifera on two morphotypes of G. ruber white ss (orange box) and sl (green box).

3. Results:

3.1 Variability of the Mg/Ca profiles

Previous studies have demonstrated significant intra-test Mg/Ca variability in planktic foraminifera (Dueñas-Bohórquez et al., 2011; Eggins et al., 2003, 2004; Hathorne et al.,

2003; Sadekov et al., 2008, 2009, 2005; Spero et al., 2015; Wit et al., 2010). These studies suggest this internal variability was probably due to ontogenic effects of Mg incorporation. Such studies highlight the importance of separating biological and environmental controls on Mg incorporation. As a consequence, in our study, three measurements were made per chamber and 2 chambers were analysed, from which we calculated average Mg/Ca per individual foraminifera. The mean chamber Mg/Ca variability was measured at ±0.26 mmol/mol (1σ). Finally, the mean variability between all measurements (six measurements in two chambers) is ±0.46 mmol/mol, which translated into a ±0.8 °C uncertainties. The overall uncertainty on temperature estimates due to propagation of analytical and calibration error is ±1 °C (Rosenthal et al., 2004).

3.2 Core-top-Holocene temperature estimates and reproducibility in both *G. ruber* white morphotypes.

The temperatures derived from Mg/Ca on the three sub-samples (a, b, c) of *G. ruber* ss in the Holocene period variance from 24 °C to 28.6 °C (±1 °C) with an average of 26.1 °C. The temperatures derived from Mg/Ca on the same subsamples of *G. ruber* sl variance from 21.9 °C to 28 °C (±1 °C) with an average of 24.5 °C (Figure 7). LA-ICP-MS mean SSTs compare well to SST from bulk *G. ruber* ss measured by ICP-AES on the same samples (Russon et al., 2010). Mean SSTs derived from LA-ICP-MS tend to be overestimated by an average of ~1 °C compared to ICP-AES, included in the error bar (±1 °C) (Table 3). We used Anova and pairwise t-tests to address the distinction between the three replicates. We find no significant differences between the temperature variance derived from Mg/Ca during the Holocene period (p value > 0.05; sub-samples a, b, c) (Table 1). However, significant and systematic differences were found between the two morphotypes of *G. ruber white* over the three replicates (p value < 0.05).

We used a Monte Carlo simulation to test our results. We conducted a t-test for all the Holocene *G. ruber* ss and sl results enabling the Mg/Ca values to vary within the uncertainty limits for 5000 iterations. Pooled *G. ruber* ss and sl samples from the Holocene were found to be significantly different 90.3 % (p value <0.05). Thus we conclude that sl morphotypes in this location appear to record cooler temperatures than the *G. ruber* ss. Such results appear to confirm the ecology and depth habitats of the

morphotypes implying that sensu stricto is a surface-water species and that sensu lato lives slightly deeper in the subsurface.

We also performed f-tests to assess the variance between the morphotypes in a similar Monte Carlo framework (n = 5000). In this case, we found no significant differences in the variance of the morphotypes (see Table 4). This result is consistent with the interpretation that despite being different morphotypes, ultimately, ecological variability within subspecies appears to be similar i.e. both morphotypes of *G. ruber* (W) appears to have similar ranges of calcification preferences, albeit at different mean temperatures.

Table 3: Sea surface temperature results derived from Mg/Ca ratio, core MD06-3018, mean and interquartile range overs 10 glacial-interglacial periods (5 interglacial (IR) and glacial (G) and two G. ruber morphotypes (ss/sl). Comparison with Russon et al., 2011 sea surface temperature estimate derived from mean Mg/Ca on G. ruber ss on the same material.

Table 4: Sea surface temperature statistical f-test results derived from Mg/Ca on two morphotypes of G. ruber (ss/sl), over the three Holocene replicate (a, b, c).

3.3 Comparison between Holocene temperature estimates and modern temperature data in both *G. ruber* white morphotypes.

We compared temperature estimates derived from Mg/Ca in individual foraminifera of *G. ruber* (ss and sl) from the Holocene period to modern datasets (Smith and Reynolds, 2004) from the sediment core location (Figure 8). Based on known ecological preferences, *G. ruber* ss is believed to reflect a surface temperature (0-30 m) and *G. ruber* sl a recorder of subsurface waters (30-75 m) (Kuroyanagi and Kawahata, 2004; Regoli et al., 2015; Wang, 2000).

The Holocene maximum estimated temperature derived from Mg/Ca in *G. ruber* (ss) corresponds to 29 °C (±1 °C) which is close to modern austral summer temperatures around 28.7 °C (±1 °C). A larger and significant offset is observed when comparing the Holocene minimum estimated temperatures, which are about 2 °C warmer than the minimum temperature in modern data. The minimum Mg/Ca temperature for the Holocene sample is estimated at 23.5 °C (±1 °C) while the modern summer corresponds to 21 °C (±1 °C).

The subsurface temperature range reconstructed from *G. ruber sl* during Holocene period varies from 21.3 to 28.2 °C (±1 °C), (Figure 8). In agreement with the temperature expected and measured in situ in the modern water column.

The mean surface and sub-surface temperature estimates derived from the Holocene sample shows an average difference of ~1.5 °C (±1 °C) compared to modern temperature records. However, no significant differences in the variance (f-test; p-values > 0.05 – see Table 4) of our Mg/Ca measurements indicate that the intra-morphotype variability in calcification temperature is the same between the ss and sl morphotypes. This would imply that, at this location, the temperature variability at the surface and subsurface ocean (i.e. where we estimate the mean calcification location is for ss and sl) is similar in the Holocene.

Figure 8: New Caledonia(23°S, 166°E) modern temperature profiles in the water Column (0-80 m). Temperature data is derived from the dataset NOAA WOA05 for the past 37 years. Blue line highlights the coldest monthly temperature and red line highlights the warmest monthly temperature in depth. Temperature data is compared with core top/Holocene estimated temperatures derived from Mg/Ca measurements of single foraminifera for the G. ruber white ss (0-30m) (orange) and G. ruber white sl (30-75m) (green).

3.4 Temperature estimates of interglacial and glacial periods recorded by both *G. ruber white* morphotypes

We compared Mg/Ca derived temperatures from *G. ruber* ss and sl for the Holocene (~0.3 ka) and Last Glacial Maximum (~22 ka; LGM) samples (Figure 9, Figure 10). The global temperature variance of surface and subsurface water temperatures estimated for the LGM period varied from 17 °C (±1 °C) to 24.8°C (±1 °C) with a mean value of 21 °C (±1 °C). Mean temperature values reconstructed from *G. ruber ss* was 22.8 °C and 20.2 °C from *G. ruber* sl. We performed Monte Carlo simulations on the LGM samples following our Holocene procedure. We found statistically significant changes ($p < 0.05$) in 95.2 % of our 5000 realizations. Overall, *G. ruber* (ss and sl) Mg/Ca-based temperatures indicate during the Holocene show temperatures around 3 °C warmer than during the LGM (Figure 9, Figure 10).

Figure 9: Interglacial (right panel) and Glacial (left panel) interquartile range (IQR) of temperature from selected periods. Comparison of the two G. ruber morphotypes: ss (orange) and sl (green). Distribution of the temperature from all interglacial periods measured (red) compared with the distribution of temperature from all glacial periods measured (blue). The Mid Pleistocene Transition, is shown by background shading using the boundary dates of Head and Gibbard (2008).

We compare MIS1/2 results with 5 other Glacial/Interglacial periods selected over the last 1.55 Ma. Temperature variance in surface and sub-surface waters slightly increases over time from 5 °C to 7 °C (maximum – minimum values derived from *G. ruber* ss and sl). The average difference of a Glacial/Interglacial cycle is ~2.5 °C with a slight progressive trend that increases over time: ~2 °C for MIS37/38 and ~3 °C for MIS1/MIS2. We observe a warming interglacial surface trend through the MPT and a cooling glacial subsurface temperature though the MPT (Figure 9).

The higher temperature recorded by *G. ruber* ss than for *G. ruber* sl is systematic for the 3 Glacial/Interglacial cycles over the last 600 ka. The mean SST difference is around 1.5°C with standard deviation of 0.7. The trend is reversed thereafter. The Mg/Ca and thus SST estimates of *G. ruber* ss are slightly lower than *G. ruber* sl during MIS 31/32 and 37, by around 0.6°C (Figure 10). No significative difference (ss-sl) were found for the MIS 31/32/37 periods ($p > 0.05$).

Figure 10: Interquartile range (IQR) of temperature during fives climatic cycles: interglacial (red boxes) and glacial (blue boxes). Comparison of the two G. ruber morphotypes: ss (orange) and sl (green). Differences between both morphotype (ss – sl) overs all selected periods (rectangle on the top panel). The time goes from right to left: the Mid Pleistocene Transition, is shown by background shading using the boundary dates of Head and Gibbard (2008).

4. Discussion:

4.1 Holocene SSTs and comparison with modern hydrographic data

We find a good correspondence between *G. ruber* core-top/Holocene temperature estimates in core MD06-3018 and modern temperature data (Figure 8). There is an overlap between modern data and estimated SSTs derived from *G. ruber* ss over the temperature variance 23-29 °C. Similarly, there is an overlap over the temperature variance: 21-28 °C for the *G. ruber* sl-based estimates. Detailed comparison shows no

temperatures are recorded below 23 °C from the *G. ruber* ss. The coldest temperautes are around 2 °C warmer than the minimum temperature recorded in modern winter condition. This observation could be explained by a number of factors discussed below.

Firstly, the age of the core top (Holocene) sample used in the study is not "modern", the ^{14}C date provides an age for the core top at 3660 years BP. As explained in the method section, the dataset used for the temperature variance of the Holocene period corresponds to the measurement of 86 individuals (Table 1; combination of the replicates a, b, c: 45 *G. ruber* ss and 45 *G. ruber* sl). Given the mean sedimentation rate of around 0.3 cm/kyr, the time integrated within 1cm of sediment deposits is estimated at around 300 years, and this is without accounting for any bioturbation effect that could mix the sedimentary signal over a longer period of time. Considering 2-5 cm of bioturbation (Teal et al 2008), the sediment layer will potentially integrate a longer period of time, around 600-1500 years. Thus, there is an age uncertainty of the "modern" core top sample which could reflect a period of slightly different temperatures 3-4000 years ago. In this case the modern temperature measurements corresponding to a monthly mean of the past 37 years are not precisely comparable with the core top temperature variance.

Secondly, differences in spatial and temporal resolution between datasets might also explain the small temperature differences between IFA and modern temperatures. The modern temperature data used here corresponds to a monthly mean during the last 37 years. Thus, the temperature data set used may not have comparable resolution as the temperature estimates from single foraminifera. Modern temperature are smoothed to the monthly resolution, whereas each individual foraminifera could provide a weekly resolved record of temperature. In order to illustrate this we compare the monthly resolved temperature data with nearby sea surface temperature records derived from *in situ* daily measurements: Uitoe data in Figure 3, near Amédée lighthouse, i.e 60 km away from the core site: see (Corrège, 2006; Varillon et al., 2018). Daily records show larger temperature variability. The amplitude of seasonal temperature variability increases by around 2 °C when using the daily resolved temperature data set. This high frequency, daily/weekly variability of water temperatures could explain some of the offsets between the estimated Holocene values and modern monthly-resolved data set.

Furthermore, low-resolution of the spatially integrated modern datasets preclude a site-specific comparison.

Considering the sediment sample, there is a possibility of reworking foraminifers due to bioturbation and thus the estimated time integrated could be even larger than 300 years. We attempted to reduce this effect by analysing an abundant species (*G. ruber*). However, we cannot exclude that there is some bioturbation and this process could have mixed foraminifera of different ages over several centimetres impacting the temperature variance measured.

Seasonal biases in ecological preferences could affect results, as previously described (Kawahata et al., 2002). Seasonal preferences in depth habitat and productivity of planktic foraminifers will skew the temperature variance estimated from a given foraminifera assemblage toward a given season and a given depth range. This effect is difficult to estimate as the mean *G. ruber* life cycle is not well constrained. For example, its life duration is estimated between a week to a month according to (Schiebel and Hemleben, 2005). This lack of precise knowledge of the species life cycles also questions the depth habitat described for each of the morphotypes, which could vary spatially and temporally. Possible seasonal vertical migration should also be considered (Figure 8) as a potential source of uncertainty.

Other factors such as salinity, carbonate chemistry [CO_2^{3-}] (Gray et al., 2018; Hönisch et al., 2013; Kısakürek et al., 2008; Lea et al., 1999; Mathien-Blard and Bassinot, 2009; Nürnberg et al., 1996), symbiont activity, ontogenetic effects and natural variability as explained in a previous section might impact Mg/Ca variability (Spero et al., 1997); (Schiebel and Hemleben, 2005); (Wit et al., 2010). Another possibility is the limitation of the calibration equation that we utilize (Dekens et al. 2002).

To summarise our findings, we observe a coherent relationship between the seasonal variance of Holocene Mg/Ca derived temperatures for both morphotypes in core MD06-3018. We observe small scale second order discrepancies between in situ and the temperature recorded by *G. ruber ss*, in order of 2 °C which we attribute as possibly reflecting a seasonal bias or a calibration effect described above. Given these encouraging results we consider justified the comparison of different

Glacial/Interglacial periods between them. This can provide information on how this temperature variability extracted from foraminifers evolves over time.

4.2 Temperature variance derived from both morphotypes during past Glacial/Interglacial periods.

4.2.1 Holocene and LGM records

The average temperature Holocene and LGM samples in this core is around 24 °C and 22°C (Russon et al. 2010). The surface temperature were derived from *G. ruber white ss* Mg/Ca measured by ICP-AES (Figure 4; Table 4). The mean SST reconstructed by LA-ICPMS compares well with the average Mg/Ca derived from ICP-AES measurements (Russon et al., 2010).

Comparison with core top/Holocene temperatures, the mean Mg/Ca-based temperatures for the LGM period are significantly colder for both surface (*G. ruber* ss) and subsurface (*G. ruber* sl) waters by around 3°C (± 1°C) (Figure 9, Figure 10). This observation is consistent with other records located in the Western Pacific Warm Pool, which show a shift of surface water mean temperature between glacial and interglacial periods of similar amplitude. Lea et al., (2000), reconstructed temperatures 2.8 °C (± 0.7 °C) colder than present during the LGM and (de Garidel-Thoron et al., 2005) observed a 3 °C (± 0.6 °C) cooling, both derived from Mg/Ca average in *G. ruber* by ICP-AES technique (de Garidel-Thoron et al., 2007).

The cooling of mean subsurface waters recorded by *G. ruber sl* morphotype during the LGM is slightly more pronounced (~3.4 °C ±1 °C) than the cooling in surface water recorded by *G. ruber ss* (~1.6 °C ±1 °C) when compared to the Holocene mean SSTs. A similar cooling of subsurface water was observed on the *G. ruber* morphotypes in a sediment core located further North in the Gulf of Papua (Regoli et al., 2015). However, the variance we observe for both morphotypes is similar for the Holocene and the LGM periods i.e. around 3 °C cooler, and confirmed by f-tests on the variance ($p > 0.05$).

The Mg/Ca variance derived temperatures in the entire water column (surface and subsurface water), from the warmest to the coldest water temperatures is around 6.9 °C

(±1 °C) for the LGM. This temperature gradient is significantly higher than that found during the Holocene (6.4 °C ±1 °C) by ~0.5 °C ($p < 0.05$). The main difference is observed for estimated *G. ruber sl* subsurface temperature which are colder temperature variability ~0.70 °C between the Holocene and the LGM. This could be interpreted as an elevation of the thermocline during the LGM. Such a result is similar to observation of (Xu et al., 2010) from a series of sediment cores investigated in the Indo Pacific Warm Pool, using surface and subsurface foraminiferal Mg/Ca.

Taken together, Holocene surface temperatures offshore New Caledonia are about 3°C warmer than during the LGM period which is of similar order as other nearby temperature reconstructions (Lea et al., 2000; Regoli et al., 2015; Stott, 2002; Visser et al., 2003). We also show that the LGM period is marked by cooler subsurface waters, which is similar to that shown by Regoli et al (2015). This change in thermal structure of the ocean seems to be a recurrent feature of the glacial period in the South West Pacific area influenced by South equatorial current and potentially by a change in the intensity of the subtropical gyre.

4.2.2 Longer-term Pleistocene evolution

We observe a systematic cooling of the surface and sub-surface temperatures during the glacial periods in comparison with interglacial (Figure 9, Figure 10). This observation is in agreement with long term temperature records of surface water (de Garidel-Thoron et al., 2005; Russon et al., 2010) and subsurface waters (Regoli et al., 2015). As in long-term SST records derived from bulk-foraminiferal Mg/Ca (Russon et al., 2010) in the study area, the average amplitude of glacial-interglacial temperatures is more larger (ie around 3 °C) for the past 400 kyr -i.e. during the 100 kyr world- than during periods prior to 900 ka (around 2 °C) - i.e. during the 40 kyr world- (Figure 4, Figure 10). Over the past fives glacial cycles, mean temperatures of subsurface waters cool from mean of 21 °C at MIS38 to mean of 22 °C at MIS2. This gradual cooling of subsurface waters has also been documented over the last 800 ka south of the Gulf of Papua (Regoli et al 2015). This study associate the subsurface cooling with an increase of variations in seasonality, from temperature variance of 4.7 °C at MIS38 to 6.3 °C at MIS2 (Figure 9). The shift occurs during and after the MPT, which might be related to proposed increases of the amplitude of obliquity (Mélice et al., 2001; Yin, 2013).

4.3 *G. ruber* morphotype temperature variance difference overs the last 1.6 Ma.

4.3.1 *G. ruber* morphotypes temperature difference during the Holocene period

Temperatures derived from *G. ruber* ss and sl morphotypes sampled from the core top sample/Holocene exhibit different Mg/Ca values (Figure 8, Figure 9, Figure 10) which we hypothesise reflect the different depths habitat that have been previously described (Wang, 2000). Our results show that *G. ruber* ss shows a systematically higher Mg/Ca ratio than *G. ruber sl* which is in agreement with this depth-habitat hypothesis. As discussed above this translates into a mean temperature offset between *G. ruber* ss and *G. ruber* sl for the Holocene period of ~1.3 °C.

This mean temperature difference between morphotypes is in agreement with previous observations using the average Mg/Ca measured by ICP-AES. (Steinke et al., 2005) that showed statistical differences of Mg/Ca ratio between *G. ruber* ss and *G. ruber* sl from sediments of the western Pacific and Indian Oceans. Present study results indicate that colder temperatures are derived from *G. ruber* sl than from *G. ruber* ss, in agreement with a subsurface habitat of *G. ruber* sl which calcifies at a greater water depth than *G. ruber* ss.

Regoli et al (2015), show that the average Mg/Ca difference for the past 3-4 ka is around 0.16 mmol/mol. In our study, we show a larger *G ruber ss* and *sl* mean offset for the Holocene around 0.3 ± 0.4 mmol/mol. Both studies show a regional change in surface water stratification and change in atmospheric climate.

It is interesting to point out that some studies document no geochemical differences between *G. ruber* ss and sl. For example, sediment trap data from the Gulf of Mexico (Thirumalai et al., 2014) or from offshore Sumatra (Mohtadi et al., 2009) showed no significant difference between *G. ruber* ss and sl Mg/Ca. These studies highlight that different locations will have different environmental conditions affecting *G. ruber* ss and sl depth habitat and, therefore, SST estimates. Thus, further calibrations of *G. ruber* morphotypes are needed with a focus on defining the variance and the factor control modern depth habitat.

4.4.2 Long-term trend evolution of *G. ruber* morphotype variations

Our observations over the past three climatic cycles spanning the last 600 ka (MIS16 to MIS1) systematically show lower mean temperature recorded by *G. ruber* sl than *G. ruber* ss. This observation support the hypothesis of a greater depth of calcification for *G. ruber* sl than *G. ruber* ss (Figure 10). However, the records derived from samples older than MIS16 show similar or even inverted temperature differences recorded by *G. ruber* ss and *G. ruber* sl (Figure 10).

One explanation for the observed variability of *G. ruber* ss-sl temperature difference over time could be explained by changes in the mixed layer depth. A deeper mixed layer, beyond the depth of life of both morphotype will promote the mixing of surface water. This hydrodynamic conditions with mixed waters between 0 and 100 meters will favour the possibility that the two morphotypes of *G. ruber* record the same variance of temperatures. In addition to the ecological factor, considering the availability of light or nutrients, the differences become insignificant and we can potentially record a reversal of trends: with *G. ruber* ss values lower than *G. ruber* sl. This variable stratification, will be site specific and could also explain the differences between published studies (Gray et al., 2018; Mohtadi et al., 2009; Thirumalai et al., 2014). These changes of the water column structure condition, that is spatially or in time will be related to variations of the hydrodynamic regime (ex: upwelling) and/or atmospheric variations (winds intensifications). This study reinforces the interest of these two populations of *G. ruber*, emphasizing that their combined but distinct use constitutes a new proxy for paleostratification.

5. Conclusion

This paper provides new data of single foraminifera laser ablation ICP-MS measurements of Mg/Ca on the two morphotypes of *G. ruber* during specific glacial interglacial cycles for the past 1.55 Ma. We observe good agreement between estimated and measured SST data. We find that discrepancies between these records might arise from potential seasonal bias on *G. ruber* ss or differences in the mean climate and

variability (seasonality and interannual variability) derived from a population of fossil specimens, in the selected periods.

We find that the average warming of surface temperature from a glacial to an interglacial periods is around 2-3 °C, over five climatic cycles. This temperature variance is in good agreement with Mg/Ca bulk-foraminiferal values measured on the same sediment core by ICP-AES in the study area (Russon et al., 2010). Our study provides further information about the seasonality over the studied periods before, during and after the Mid-Pleistocene Transition. We observe an increase of ~1.5 °C in interglacial surface water temperature and a decrease of ~2 °C in glacial subsurface water, a finding consistent with the increase in the amplitude of climatic cycles during MPT.

Finally, this study shows that the morphotypes of *G. ruber ss* and *sl* record different Mg/Ca values corresponding to different water temperature in agreement with their depth habitat, at our site location. The analysis of morphotypes living at different water depth shows the potential to reconstruct water masses' stratification in paleo-climate studies. We observe a shift in stratification between MIS16 and MIS31. We interpret this long-term evolution of differences in *G. ruber* ss/sl derived SSTS as reflecting modification of the water column stratification around the MPT in the South Pacific offshore New Caledonia.

Acknowledgements

Thanks to the detailed comments of the reviewers who greatly improved this paper. We thank Tom Russon for his work already done on this area and on the samples of this core. Thank you also for his first statistical expertise on our data.
We finally thank our funding sources: TOTAL and IFREMER.

References

Anand, P., Elderfield, H., Conte, M.H., 2003. Calibration of Mg/Ca thermometry in planktonic foraminifera from a sediment trap time series. Paleoceanography 18, 1050. https://doi.org/10.1029/2002PA000846

Barker, S., Greaves, M., Elderfield, H., 2003. A study of cleaning procedures used for foraminiferal Mg/Ca paleothermometry. Geochem. Geophys. Geosystems 4, 8407.

https://doi.org/10.1029/2003GC000559

Behringer, D., Xue, Y., 2004. Evaluation of the global ocena data assimilation system at NCEP: The Pacific Ocean 6.

Bijma, J., Faber, W.W.J., Hemleben, C., 1990. Temperature and salinity limits for growth and survival of some planktonic foraminifers in laboratory cultures. J. Foraminifer. Res. 20, 95–116.

Billups, K., Spero, H.J., 1996. Reconstructing the stable isotope geochemistry and paleotemperatures of the equatorial Atlantic during the last 150,000 years: Results from individual foraminifera. Paleoceanography 11, 217–238. https://doi.org/10.1029/95PA03773

Bostock, H.C., Opdyke, B.N., Gagan, M.K., Kiss, A.E., Fifield, L.K., 2006. Glacial/interglacial changes in the East Australian current. Clim. Dyn. 26, 645–659. https://doi.org/10.1007/s00382-005-0103-7

Corrège, T., 2006. Sea surface temperature and salinity reconstruction from coral geochemical tracers. Palaeogeogr. Palaeoclimatol. Palaeoecol. 232, 408–428. https://doi.org/10.1016/j.palaeo.2005.10.014

de Garidel-Thoron, Rosenthal, Y., Bassinot, F., Beaufort, L., 2005. Stable sea surface temperatures in the western Pacific warm pool over the past 1.75 million years. Nature 433, 294–298. https://doi.org/10.1038/nature03273

de Garidel-Thoron, T., 2002. Dynamique climatique de l'Océan Pacifique ouest équatorial au cours du Pléistocène récent. Université de droit, d'économie et des sciences-Aix-Marseille III.

de Garidel-Thoron, T., Rosenthal, Y., Beaufort, L., Bard, E., Sonzogni, C., Mix, A.C., 2007. A multiproxy assessment of the western equatorial Pacific hydrography during the last 30 kyr: degalcail Equatorial Pacific hydrography. Paleoceanography 22, PA3204. https://doi.org/10.1029/2006PA001269

de Villiers, S., Greaves, M., Elderfield, H., 2002. An intensity ratio calibration method for the accurate determination of Mg/Ca and Sr/Ca of marine carbonates by ICP-AES. Geochem. Geophys. Geosystems 3, 1001. https://doi.org/10.1029/2001GC000169

Dekens, P.S., Lea, D.W., Pak, D.K., Spero, H.J., 2002. Core top calibration of Mg/Ca in tropical foraminifera: Refining paleotemperature estimation: Core top calibration. Geochem. Geophys. Geosystems 3, 1–29. https://doi.org/10.1029/2001GC000200

Delcroix, T., Lenormand, O., 1997. ENSO signals in the vicinity of New Caledonia, South Western Pacific. Ocean. Acta 20, 481–491.

Dueñas-Bohórquez, A., da Rocha, R.E., Kuroyanagi, A., de Nooijer, L.J., Bijma, J., Reichart, G.-J., 2011. Interindividual variability and ontogenetic effects on Mg and Sr incorporation in the planktonic foraminifer Globigerinoides sacculifer. Geochim. Cosmochim. Acta 75, 520–532. https://doi.org/10.1016/j.gca.2010.10.006

Eggins, S., De Deckker, P., Marshall, J., 2003. Mg/Ca variation in planktonic foraminifera tests: implications for reconstructing palaeo-seawater temperature and habitat migration. Earth Planet. Sci. Lett. 212, 291–306. https://doi.org/10.1016/S0012-821X(03)00283-8

Eggins, S., Sadekov, A., Dedeckker, P., 2004. Modulation and daily banding of Mg/Ca in tests by symbiont photosynthesis and respiration: a complication for seawater thermometry? Earth Planet. Sci. Lett. 225, 411–419. https://doi.org/10.1016/j.epsl.2004.06.019

Elderfield, H., Ganssen, G., 2000. Past temperature and δ18O of surface ocean waters inferred from foraminiferal Mg/Ca ratios. Nature 405, 442–445.

Fairbanks, R.G., Sverdlove, M., Free, R., Wiebe, P.H., Bé, A.W.H., 1982. Vertical distribution and isotopic fractionation of living planktonic foraminifera from the Panama Bassin. Nature 298.

Gray, W.R., Weldeab, S., Lea, D.W., Rosenthal, Y., Gruber, N., Donner, B., Fischer, G., 2018. The effects of temperature, salinity, and the carbonate system on Mg/Ca in Globigerinoides ruber (white): A global sediment trap calibration. Earth Planet. Sci. Lett. 482, 607–620. https://doi.org/10.1016/j.epsl.2017.11.026

Hathorne, E.C., Alard, O., James, R.H., Rogers, N.W., 2003. Determination of intratest variability of trace elements in foraminifera by laser ablation inductively coupled plasma-mass spectrometry: Trace elements in foraminifera. Geochem. Geophys. Geosystems 4, 8408. https://doi.org/10.1029/2003GC000539

Hathorne, E.C., James, R.H., Savage, P., Alard, O., 2008. Physical and chemical characteristics of particles produced by laser ablation of biogenic calcium carbonate. J Anal Spectrom 23, 240–243. https://doi.org/10.1039/B706727E

Hönisch, B., Allen, K.A., Lea, D.W., Spero, H.J., Eggins, S.M., Arbuszewski, J., deMenocal, P., Rosenthal, Y., Russell, A.D., Elderfield, H., 2013. The influence of salinity on Mg/Ca in planktic foraminifers – Evidence from cultures, core-top sediments and complementary δ18O. Geochim. Cosmochim. Acta 121, 196–213. https://doi.org/10.1016/j.gca.2013.07.028

Jochum, K.P., Weis, U., Stoll, B., Kuzmin, D., Yang, Q., Raczek, I., Jacob, D.E., Stracke, A., Birbaum, K., Frick, D.A., Günther, D., Enzweiler, J., 2011. Determination of Reference

Values for NIST SRM 610-617 Glasses Following ISO Guidelines. Geostand. Geoanalytical Res. 35, 397–429. https://doi.org/10.1111/j.1751-908X.2011.00120.x

Kawahata, H., Nishimura, A., Gagan, M.K., 2002. Seasonal change in foraminiferal production in the western equatorial Pacific warm pool: evidence from sediment trap experiments. Deep Sea Res. Part II Top. Stud. Oceanogr. 49, 2783–2800.

Kısakürek, B., Eisenhauer, A., Böhm, F., Garbe-Schönberg, D., Erez, J., 2008. Controls on shell Mg/Ca and Sr/Ca in cultured planktonic foraminiferan, Globigerinoides ruber (white). Earth Planet. Sci. Lett. 273, 260–269. https://doi.org/10.1016/j.epsl.2008.06.026

Koho, K.A., de Nooijer, L.J., Fontanier, C., Toyofuku, T., Oguri, K., Kitazato, H., Reichart, G.-J., 2017. Benthic foraminiferal Mn / Ca ratios reflect microhabitat preferences. Biogeosciences 14, 3067–3082. https://doi.org/10.5194/bg-14-3067-2017

Kuroyanagi, A., Kawahata, H., 2004. Vertical distribution of living planktonic foraminifera in the seas around Japan. Mar. Micropaleontol. 53, 173–196. https://doi.org/10.1016/j.marmicro.2004.06.001

Lea, D.W., Mashiotta, T.A., Spero, H.J., 1999. Controls on magnesium and strontium uptake in planktonic foraminifera determined by live culturing. Geochim. Cosmochim. Acta 63, 2369–2379.

Lea, D.W., Pak, D.K., Spero, H.J., 2000. Climate impact of late Quaternary equatorial Pacific sea surface temperature variations. Science 289, 1719–1724.

Leduc, G., Vidal, L., Cartapanis, O., Bard, E., 2009. Modes of eastern equatorial Pacific thermocline variability: Implications for ENSO dynamics over the last glacial period: ENSO dynamics over the last 50 ka. Paleoceanography 24, PA3202. https://doi.org/10.1029/2008PA001701

Mathien-Blard, E., Bassinot, F., 2009. Salinity bias on the foraminifera Mg/Ca thermometry: Correction procedure and implications for past ocean hydrographic reconstructions: salinity bias on G. ruber Mg thermometry. Geochem. Geophys. Geosystems 10, Q12011. https://doi.org/10.1029/2008GC002353

Mélice, J.L., Coron, A., Berger, A., 2001. Amplitude and Frequency Modulations of the Earth's Obliquity for the Last Million Years. J. Clim. 14, 1043–1054. https://doi.org/10.1175/1520-0442(2001)014<1043:AAFMOT>2.0.CO;2

Mohtadi, M., Steinke, S., Groeneveld, J., Fink, H.G., Rixen, T., Hebbeln, D., Donner, B., Herunadi, B., 2009. Low-latitude control on seasonal and interannual changes in planktonic foraminiferal flux and shell geochemistry off south Java: A sediment trap study. Paleoceanography 24, PA1201. https://doi.org/10.1029/2008PA001636

Nürnberg, D., Bijma, J., Hemleben, C., 1996. Assessing the reliability of magnesium in foraminiferal calcite as a proxy for water mass temperatures. Geochim. Cosmochim. Acta 60, 803–814.

Petersen, J., Barras, C., Bézos, A., La, C., de Nooijer, L.J., Meysman, F.J.R., Mouret, A., Slomp, C.P., Jorissen, F.J., 2017. Mn/Ca intra-test variability in the benthic foraminifer: Ammonia tepida. Biogeosciences Discuss. 1–37. https://doi.org/10.5194/bg-2017-273

Regoli, F., de Garidel-Thoron, T., Tachikawa, K., Jian, Z., Ye, L., Droxler, A.W., Lenoir, G., Crucifix, M., Barbarin, N., Beaufort, L., 2015. Progressive shoaling of the equatorial Pacific thermocline over the last eight glacial periods: Pacific thermocline shoaling over 800 ka. Paleoceanography 30, 439–455. https://doi.org/10.1002/2014PA002696

Reynolds, R.W., Rayner, N.A., Smith, T.M., Stokes, D.C., Wang, W., 2002. An Improved In Situ and Satellite SST Analysis for Climate. J. Clim. 15, 17.

Ridgway, K.R., Dunn, J.R., 2003. Mesoscale structure of the mean East Australian Current System and its relationship with topography. Prog. Oceanogr. 56, 189–222. https://doi.org/10.1016/S0079-6611(03)00004-1

Rosenthal, Y., Lohmann, G.P., Lohmann, K.C., Sherrell, R.M., 2000. Incorporation and preservation of Mg in Globigerinoides sacculifer:Implications for reconstructing the temperature and of seawater. Paleoceanography 15, 11.

Rosenthal, Y., Perron-Cashman, S., Lear, C.H., Bard, E., Barker, S., Billups, K., Bryan, M., Delaney, M.L., deMenocal, P.B., Dwyer, G.S., Elderfield, H., German, C.R., Greaves, M., Lea, D.W., Marchitto, T.M., Pak, D.K., Paradis, G.L., Russell, A.D., Schneider, R.R., Scheiderich, K., Stott, L., Tachikawa, K., Tappa, E., Thunell, R., Wara, M., Weldeab, S., Wilson, P.A., 2004. Interlaboratory comparison study of Mg/Ca and Sr/Ca measurements in planktonic foraminifera for paleoceanographic research: MEASUREMENTS IN PLANKTONIC FORAMINIFERA. Geochem. Geophys. Geosystems 5, 1–29. https://doi.org/10.1029/2003GC000650

Russon, T., Elliot, M., Sadekov, A., Cabioch, G., Corrège, T., De Deckker, P., 2010. Inter-hemispheric asymmetry in the early Pleistocene Pacific warm pool: Pacific Warm Pool evolution. Geophys. Res. Lett. 37, L11601. https://doi.org/10.1029/2010GL043191

Russon, T.F., 2011. Paleoceanography of the southern Coral Sea across the Mid-Pleistocene Transition.

Sadekov, A., Eggins, S.M., De Deckker, P., Kroon, D., 2008. Uncertainties in seawater thermometry deriving from intratest and intertest Mg/Ca variability in Globigerinoides ruber. Paleoceanography 23, PA1215. https://doi.org/10.1029/2007PA001452

Sadekov, A., Eggins, S.M., De Deckker, P., Ninnemann, U., Kuhnt, W., Bassinot, F., 2009. Surface and subsurface seawater temperature reconstruction using Mg/Ca microanalysis of planktonic foraminifera Globigerinoides ruber, Globigerinoides sacculifer, and Pulleniatina obliquiloculata. Paleoceanography 24, PA3201. https://doi.org/10.1029/2008PA001664

Sadekov, A.Y., Eggins, S.M., De Deckker, P., 2005. Characterization of Mg/Ca distributions in planktonic foraminifera species by electron microprobe mapping: Mg/Ca in planktonic foraminifera. Geochem. Geophys. Geosystems 6, Q12P06. https://doi.org/10.1029/2005GC000973

Schiebel, R., Hemleben, C., 2005. Modern planktic foraminifera. Paläontol. Z. 79, 135–148. https://doi.org/10.1007/BF03021758

Smith, T.M., Reynolds, R.W., 2004. Improved Extended Reconstruction of SST (1854–1997). J. Clim. 17, 2466–2477. https://doi.org/10.1175/1520-0442(2004)017<2466:IEROS>2.0.CO;2

Spero, H.J., Barth, J.V., Wintterlin, J., Ertl, G., 1997. Complex pathways in dissociative adsorption of oxygen on platinum. Nature 390, 495–497.

Spero, H.J., Eggins, S.M., Russell, A.D., Vetter, L., Kilburn, M.R., Hönisch, B., 2015. Timing and mechanism for intratest Mg/Ca variability in a living planktic foraminifer. Earth Planet. Sci. Lett. 409, 32–42. https://doi.org/10.1016/j.epsl.2014.10.030

Steinke, S., Chiu, H.-Y., Yu, P.-S., Shen, C.-C., Löwemark, L., Mii, H.-S., Chen, M.-T., 2005. Mg/Ca ratios of two Globigerinoides ruber (white) morphotypes: Implications for reconstructing past tropical/subtropical surface water conditions: G. ruber (white) Mg/Ca ratio. Geochem. Geophys. Geosystems 6, Q11005. https://doi.org/10.1029/2005GC000926

Stott, L., 2002. Super ENSO and Global Climate Oscillations at Millennial Time Scales. Science 297, 222–226. https://doi.org/10.1126/science.1071627

Thirumalai, K., Partin, J.W., Jackson, C.S., Quinn, T.M., 2013. Statistical constraints on El Niño Southern Oscillation reconstructions using individual foraminifera: A sensitivity analysis: IFA-ENSO UNCERTAINTY. Paleoceanography 28, 401–412. https://doi.org/10.1002/palo.20037

Thirumalai, K., Quinn, T.M., Okumura, Y., Richey, J.N., Partin, J.W., Poore, R.Z., Moreno-Chamarro, E., 2018. Pronounced centennial-scale Atlantic Ocean climate variability correlated with Western Hemisphere hydroclimate. Nat. Commun. 9. https://doi.org/10.1038/s41467-018-02846-4

Thirumalai, K., Richey, J.N., Quinn, T.M., Poore, R.Z., 2014. Globigerinoides ruber morphotypes in the Gulf of Mexico: A test of null hypothesis. Sci. Rep. 4. https://doi.org/10.1038/srep06018

Varillon, D., Fiat, S., Magron, F., Allenbach, M., Hoibian, T., De Ramon N'Yeurt, A., Ganachaud, A., Aucan, J., Pelletier, B., Hocdé, R., 2018. ReefTEMPS : the observation network of the coastal sea waters of the South, West and South-West Pacific. https://doi.org/10.17882/55128

Visser, K., Thunell, R., Stott, L., 2003. Magnitude and timing of temperature change in the Indo-Pacific warm pool during deglaciation. Nature 421, 152–155. https://doi.org/10.1038/nature01297

Wang, L., 2000. Isotopic signals in two morphotypes of Globigerinoides ruber (white) from the South China Sea: implications for monsoon climate change during the last glacial cycle. Palaeogeogr. Palaeoclimatol. Palaeoecol. 161, 381–394.

Wit, J.C., Reichart, G.-J., A Jung, S.J., Kroon, D., 2010. Approaches to unravel seasonality in sea surface temperatures using paired single-specimen foraminiferal δ18O and Mg/Ca analyses: Paleoceanography 25, PA4220. https://doi.org/10.1029/2009PA001857

Xu, J., Kuhnt, W., Holbourn, A., Regenberg, M., Andersen, N., 2010. Indo-Pacific Warm Pool variability during the Holocene and Last Glacial Maximum. Paleoceanography 25, PA4230. https://doi.org/10.1029/2010PA001934

Yin, Q., 2013. Insolation-induced mid-Brunhes transition in Southern Ocean ventilation and deep-ocean temperature. Nature 494, 222.

Žarić, S., Schulz, M., Mulitza, S., 2005. Global prediction of planktic foraminiferal fluxes from hydrographic and productivity data 48.

Figures and Tables

Figure 1: Modern hydrodynamic surface water in New Caledonia. Present-day seasonal climatology in the New Caledonia core location (NOAA, WOA05): surface temperature (0m) during a. austral winter (August) b. austral summer (February) with Schematic surface water circulation regimes in the subtropical southwest Pacific. Abbreviations are as follows: SEC = South Equatorial Current, EAC = East Australian Current, SCJ = South Caledonian Jet.

Figure 2: Potential Temperature profile and Salinity profile (0-200m), mean of the last 37 years, at the core location per month and depth (dotted black line) from NOAA, (GOAS). Red points correspond to the mean mixed layer depth during austral summer (40m) and austral winter (130m).

Figure 3: Daily and monthly sea surface temperature data at 5m depth since 1992 to 2001 from Uitoé.

Figure 4: Oxygen Isotope (black) and Sea Surface Temperature (SST) (bleu) derived from Mg/Ca measurement on planktic foraminifera G. ruber white ss core MD06-3018 (adapted from Russon et al 2010). Marin Stage Isotopes (MIS) interpretation and samples selection position (red points) in both curves overs last 1.6 Ma. The Mid Pleistocene Transition (MPT) interval, is shown by background shading using the boundary dates of Head and Gibbard (2008).

Figure 5: G. ruber white sensu stricto (ss) and sensu lato (sl) foraminifera defined by Wang et al, (2000) terminology, SEM picture from the core MD06-3018, after laser ablation measurement.

Figure 6: Typical G. ruber trace elements (Mg, Ca, Mn, Fe, Al and Ba) raw profiles in counts from laser ablation across one hole in one chamber. All tests have been ablated (profiled) from the outer to the inner surface (left to right).

Figure 7: Reproducibility of the Holocene period with 3 replicates (a,b,c). Interquartile range of sea surface temperature (SST) derived from Mg/Ca in single foraminifera on two morphotypes of G. ruber white ss (orange box) and sl (green box).

Figure 8: New Caledonia(23°S, 166°E) modern temperature profiles in the water Column (0-80 m). Temperature data is derived from the dataset NOAA WOA05 for the past 37 years. Blue line highlights the coldest monthly temperature and red line

highlights the warmest monthly temperature in depth. Temperature data is compared with core top/Holocene estimated temperatures derived from Mg/Ca measurements of single foraminifera for the G. ruber white ss (0-30m) (orange) and G. ruber white sl (30-75m) (green).

Figure 9: Interglacial (right panel) and Glacial (left panel) interquartile range (IQR) of temperature from selected periods. Comparison of the two G. ruber morphotypes: ss (orange) and sl (green). Distribution of the temperature from all interglacial periods measured (red) compared with the distribution of temperature from all glacial periods measured (blue). The Mid Pleistocene Transition, is shown by background shading using the boundary dates of Head and Gibbard (2008).

Figure 10: Interquartile range (IQR) of temperature during fives climatic cycles: interglacial (red boxes) and glacial (blue boxes). Comparison of the two G. ruber morphotypes: ss (orange) and sl (green). Differences between both morphotype (ss – sl) overs all selected periods (rectangle on the top panel). The time goes from right to left: the Mid Pleistocene Transition, is shown by background shading using the boundary dates of Head and Gibbard (2008).

Table 1 : Samples selection and LA-ICP-MS in single foraminifera measurement strategy, core MD06-3018. Corresponding marine isotope stage (MIS), depth of samples from which foraminifera were picked, corresponding age in ka, Glacial (G) or Interglacial period (IG), number of foraminifera G. ruber ss and G. ruber sl analysed per level, number of chambers and number of measurements per chamber analysed and finally the total number of ablations per level.

Table 2: Summarized LA-ICP-MS operating conditions for technic.

Table 3: Sea surface temperature results derived from Mg/Ca ratio, core MD06-3018, mean and interquartile range overs 10 glacial-interglacial periods (5 interglacial (IR) and glacial (G) and two G. ruber morphotypes (ss/sl). Comparison with Russon et al., 2011 sea surface temperature estimate derived from mean Mg/Ca on G. ruber ss on the same material.

Table 4: Sea surface temperature statistical f-test results derived from Mg/Ca on two morphotypes of G. ruber (ss/sl), over the three Holocene replicate (a, b, c).

Table 1: Samples selection and LA-ICP-MS in single foraminifera measurement strategy core MD06-3018

Sample	Depth in core (cm)	Age (ka)	Period	number of *G.ruber* ss measured	number of *G.ruber* sl measured	number of chambers measured */G.ruber*	number of measurement /chambers	number of hole /LA
MIS1-a	1	0.3	IG	13	13	2	3	156
MIS1-b	1	0.3	IG	15	15	2	3	180
MIS1-c	1	0.3	IG	15	15	2	3	180
MIS2	75	22	G	15	15	2	3	180
MIS11	990	405	IG	15	15	2	3	180
MIS12	1050	435	G	15	15	2	3	180
MIS15	1300	607	IG	15	15	2	3	180
MIS16	1330	630	G	15	15	2	3	180
MIS31	1880	1069	IG	15	15	2	3	180
MIS32	1950	1095	G	15	15	2	3	180
MIS37	2083	1235	IG	15	15	2	3	180
MIS38	2085	1250	G	15	15	2	3	180

Table 2: Summarised LA-ICP-MS operating conditions for technic

Analyte G2 laser ablation system (193 nm)	
Energy density Laser fluence	0.91 J/cm2
Laser pulse repetition rate	4 Hz
He flow rates	0.7 and 0.3 LPM
Projected spot size	65 µm
Quadrupole Varian 820-MS	
Dwell time	20 ms
RF power	1.15 kw
Sheath gas flow	0.8-0.9 L/min
232Th16O+/232Th+	< 0.5%
U/Th	~1
Limite quantification	ET*10
Limite detection	ET*3

only those that remain constant throughout all the experiments are presented here.

Table 3: Sea surface temperature results derived from Mg/Ca ratio, core MD06-3018

Samples	Age	Stage	Period	Morphotype	mean Mg/Ca	STD	mean SST	STD	min	Q1	median	Q3	max	Russon et al., 2011 SST estimation
cm	ka	MIS	IG/G	ss/sl	mmol/mol	mmol/mol	°C	°C	°C	°C	°C	°C	°C	°C
1_2	0.3	MIS1	IG	sl	4.66	0.82	24.34	1.88	21.93	22.81	24.54	25.26	28.00	NA
1_2	0.3	MIS1	IG	ss	5.56	0.71	26.37	1.42	24.07	25.48	26.07	27.67	28.61	24.40
75_76	22	MIS2	G	sl	3.26	0.55	20.38	1.88	17.03	19.13	20.21	21.96	23.39	NA
75_76	22	MIS2	G	ss	4.00	0.48	22.71	1.35	19.78	21.88	22.79	23.51	24.84	22.18
990_991	405	MIS11	IG	sl	4.38	0.74	23.65	1.91	19.52	22.37	23.80	24.98	27.00	NA
990_991	405	MIS11	IG	ss	4.75	0.75	24.57	1.74	22.05	23.19	24.84	25.84	27.82	24.33
1050_1051	435	MIS12	G	sl	3.78	0.67	22.01	1.95	18.75	20.65	22.20	23.51	25.86	NA
1050_1051	435	MIS12	G	ss	3.96	0.53	22.59	1.46	20.42	21.55	22.74	23.67	25.65	23.01
1300_1301	607	MIS15	IG	sl	4.69	0.40	24.52	0.94	23.36	23.70	24.36	25.30	26.19	NA
1300_1301	607	MIS15	IG	ss	5.44	0.73	26.11	1.49	24.20	25.43	26.17	27.21	29.04	23.74
1330_1331	630	MIS16	G	sl	4.05	0.66	22.80	1.85	19.52	21.36	23.10	24.22	25.41	NA
1330	63	MI	G	ss	4.58	0.52	24	1.	22	23	24.	25	26	22.07

_1331	0	S16					.24	29	.96	.68	42	.16	.13	
1880_1881	1069	MIS31	IG	sl	5.27	0.43	25.83	0.91	24.56	25.05	25.54	26.75	27.04	NA
1880_1881	1069	MIS31	IG	ss	5.05	0.77	25.27	1.69	22.51	23.77	24.89	26.48	28.29	24.24
1950_1951	1095	MIS32	G	sl	4.01	0.42	22.78	1.15	21.05	22.02	22.71	23.12	24.77	NA
1950_1951	1095	MIS32	G	ss	4.15	0.77	23.04	2.01	19.89	21.82	22.57	24.01	26.33	22.58
2100_2001	1235	MIS37	IG	sl	4.77	0.65	24.64	1.58	20.89	23.74	24.59	25.81	26.61	NA
2100_2001	1235	MIS37	IG	ss	4.72	0.46	24.58	1.06	23.26	23.68	24.23	25.40	26.59	22.77
2130_2131	1250	MIS38	G	sl	3.71	0.44	21.89	1.33	19.41	21.25	21.87	22.54	24.13	NA
2130_2131	1250	MIS38	G	ss	4.10	0.33	23.03	0.91	21.69	22.60	23.22	23.47	24.44	21.64

Table 4: Sea surface temperature statistical f-test results derived from Mg/Ca on two morphotypes of *G. ruber* (ss/sl), over the three Holocene replicates (a, b, c).

Holocene

f-test	MIS1a-SS	MIS1b-SS	MIS1c-SS	MIS1a-SL	MIS1b-SL	MIS1c-SL
MIS1a-SS	-	*p*=0.77	*p*=0.71	*p*=0.45	*p*=0.50	*p*=0.38
MIS1b-SS	-	-	*p*=0.48	*p*=0.27	*p*=0.3	*p*=0.22
MIS1c-SS	-	-	-	*p*=0.68	*p*=0.75	*p*=0.60
MIS1a-SL	-	-	-	-	*p*=0.92	*p*=0.91
MIS1b-SL	-	-	-	-	-	*p*=0.84
MIS1c-SL	-	-	-	-	-	-

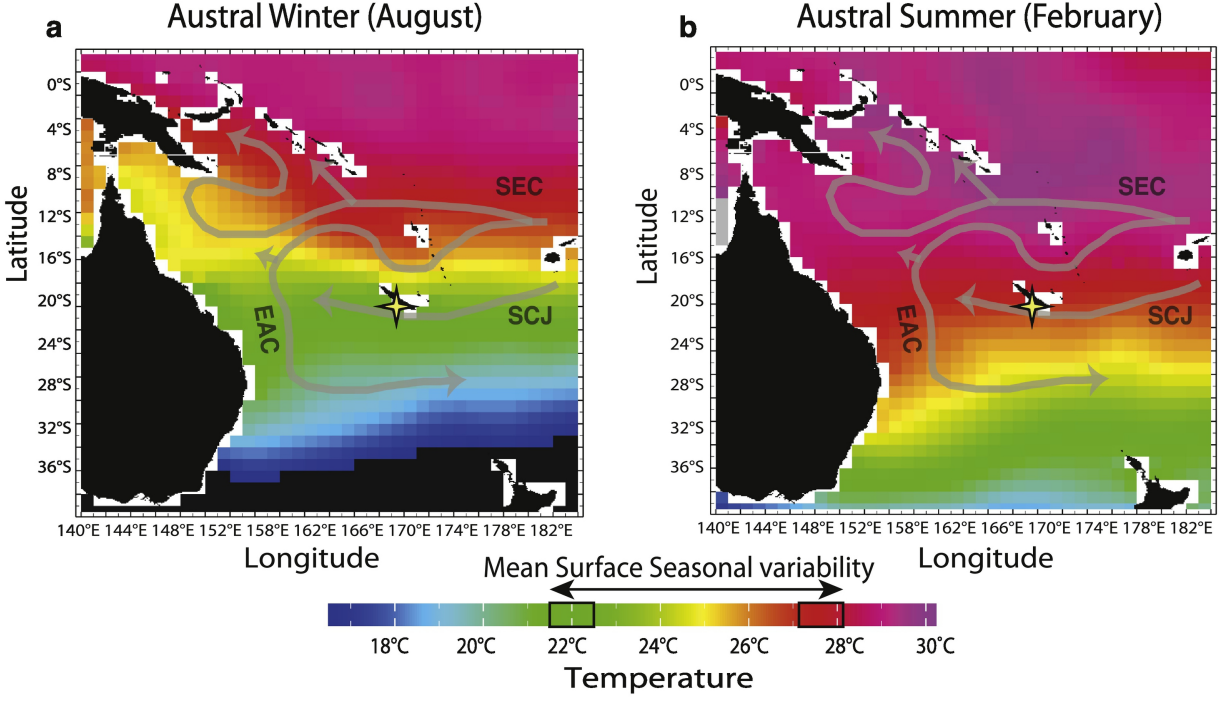
a
Austral Winter (August)
b
Austral Summer (February)
Latitude
Longitude
0°S
4°S
8°S
12°S
16°S
20°S
24°S
28°S
32°S
36°S
140°E 144°E 148°E 152°E 158°E 162°E 166°E 170°E 174°E 178°E 182°E
SEC
SCJ
EAC
Mean Surface Seasonal variability
18°C
20°C
22°C
24°C
26°C
28°C
30°C
Temperature

Figure 1

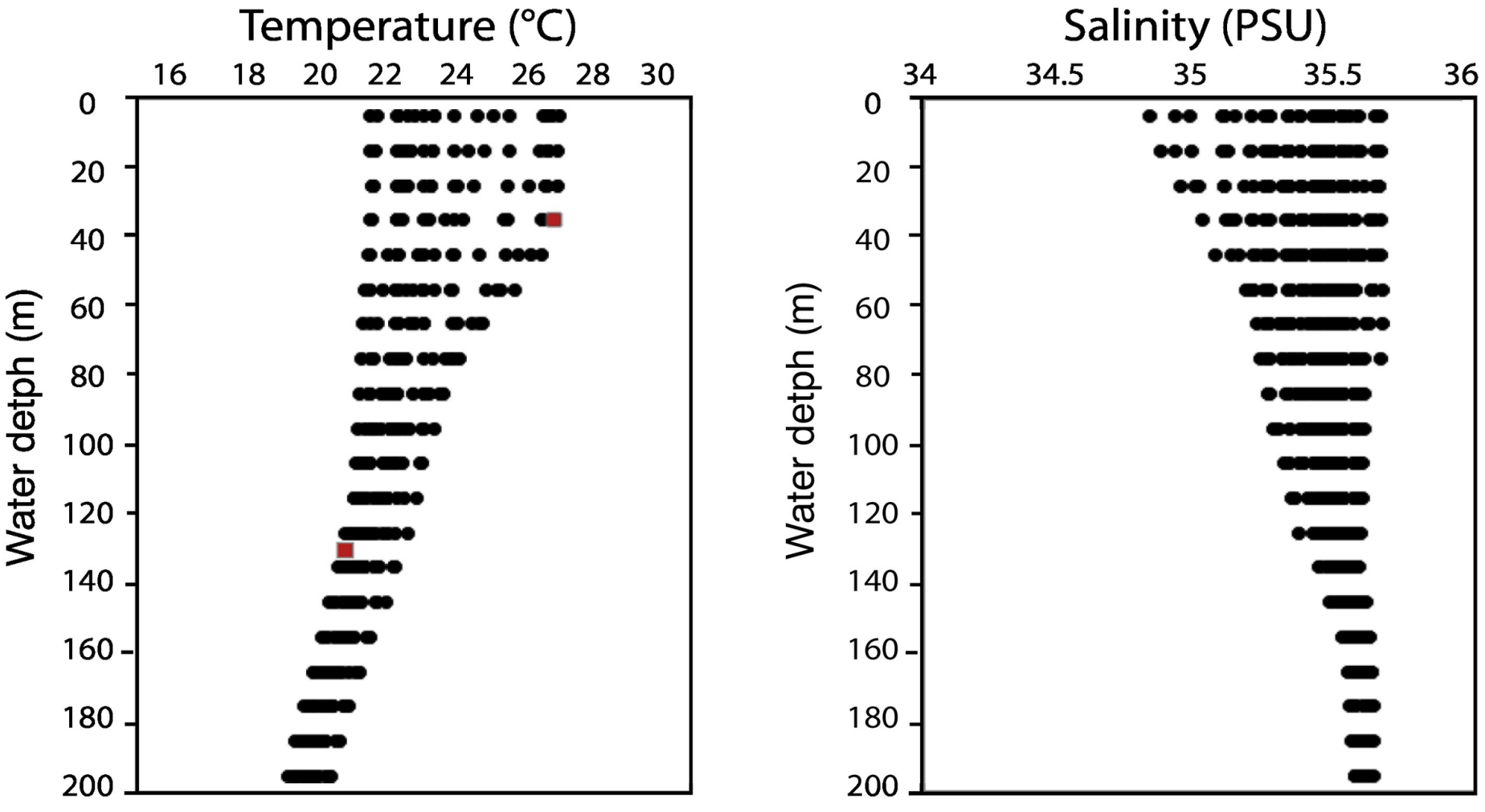
Temperature (°C)
16
18
20
22
24
26
28
30
Salinity (PSU)
34
34.5
35
35.5
36
Water detph (m)
0
20
40
60
80
100
120
140
160
180
200

Figure 2

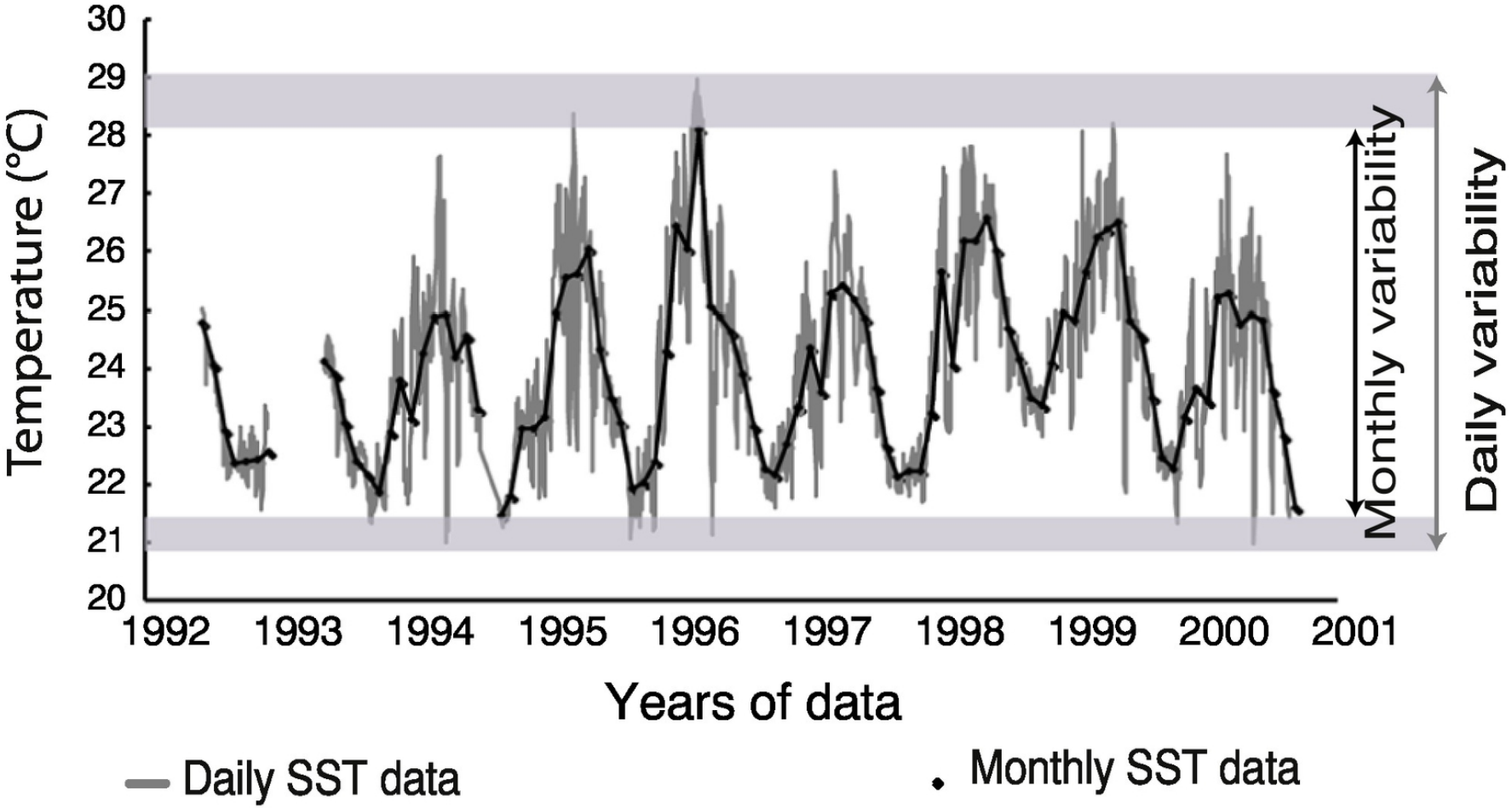
Temperature (°C)
30
29
28
27
26
25
24
23
22
21
20
1992
1993
1994
1995
1996
1997
1998
1999
2000
2001
Years of data
Monthly variability
Daily variability
Daily SST data
Monthly SST data

Figure 3

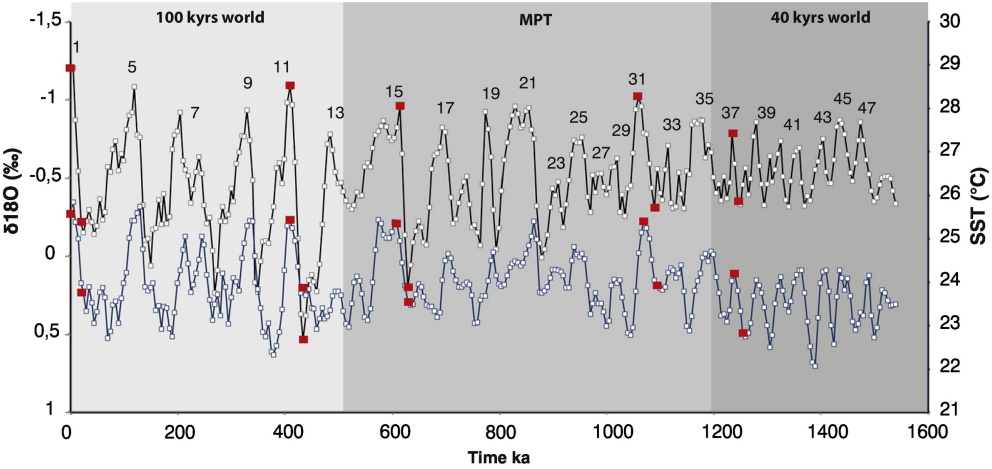
100 kyrs world
MPT
40 kyrs world
δ18O (‰)
SST (°C)
Time ka
-1,5
-1
-0,5
0
0,5
1
30
29
28
27
26
25
24
23
22
21
0
200
400
600
800
1000
1200
1400
1600
1
5
7
9
11
13
15
17
19
21
23
25
27
29
31
33
35
37
39
41
43
45
47

Figure 4

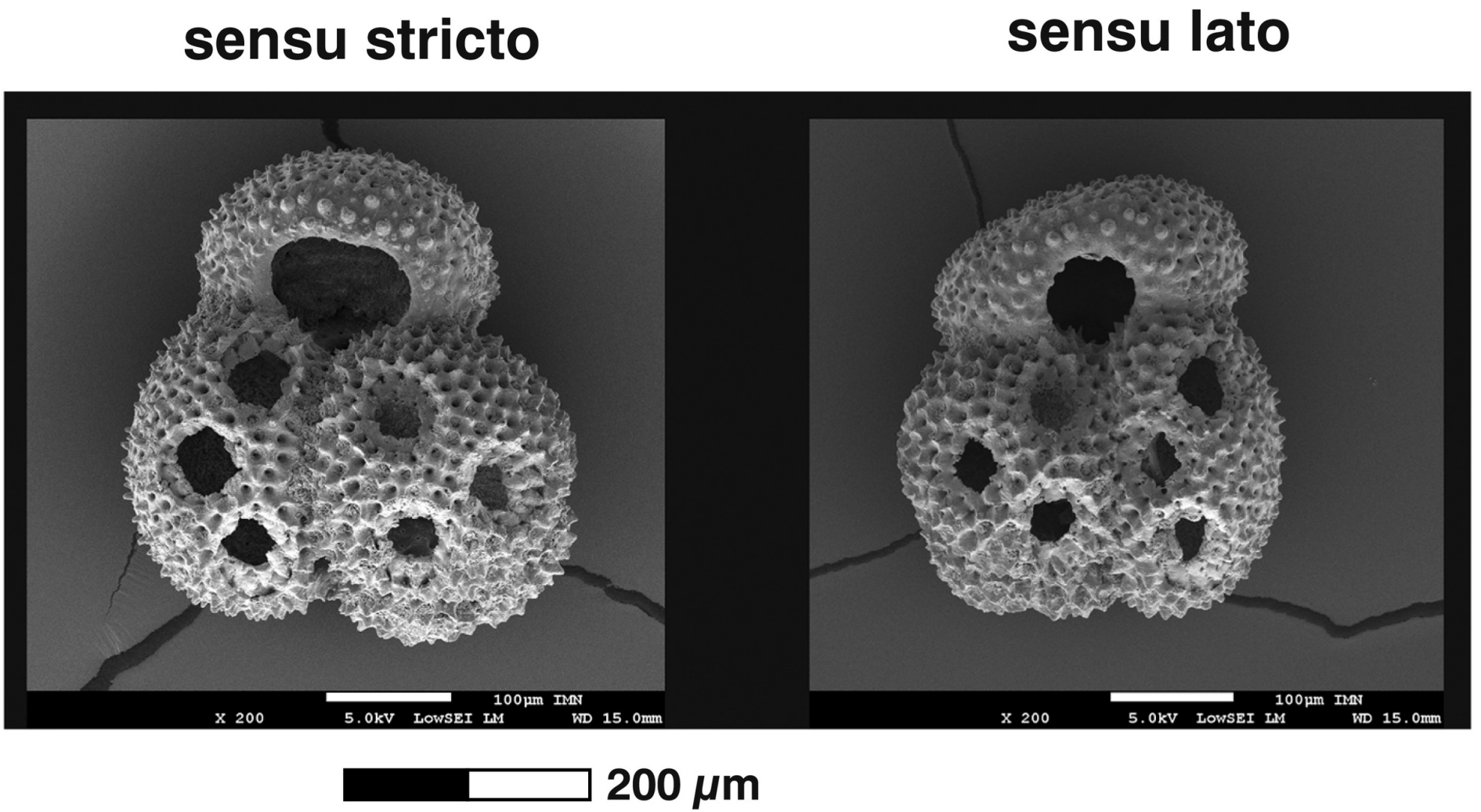
sensu stricto
sensu lato
100µm IMN
X 200 5.0kV LowSEI LM WD 15.0mm
100µm IMN
X 200 5.0kV LowSEI LM WD 15.0mm
200 µm

Figure 5

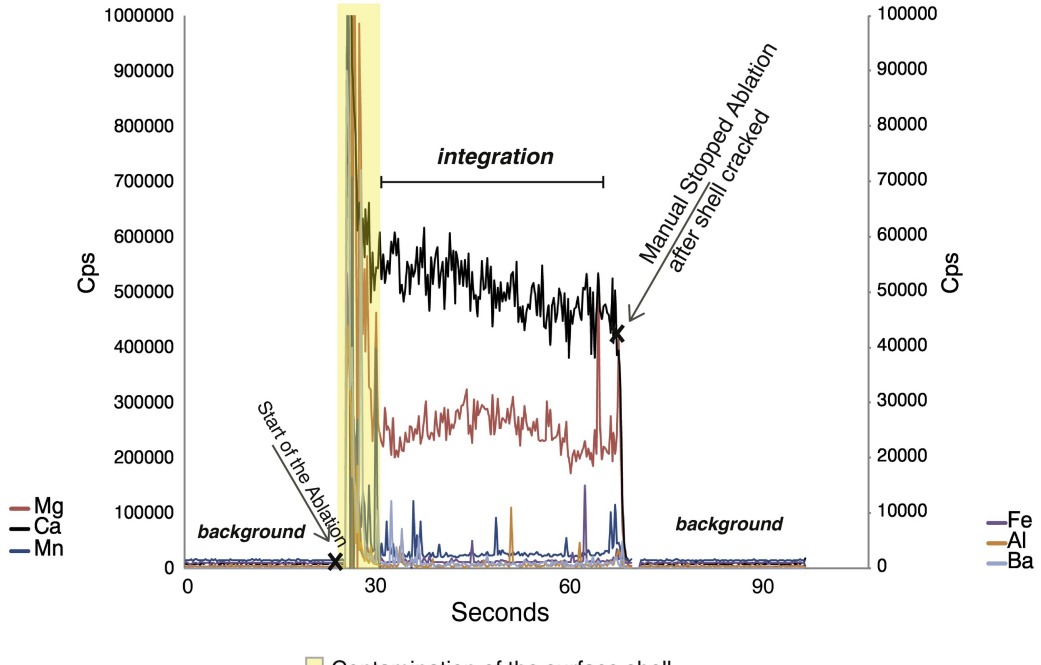
1000000
900000
800000
700000
600000
500000
400000
300000
200000
100000
0
Cps
100000
90000
80000
70000
60000
50000
40000
30000
20000
10000
0
Cps
integration
Manual Stopped Ablation
after shell cracked
Start of the Ablation
background
background
Mg
Ca
Mn
Fe
Al
Ba
0
30
60
90
Seconds
Contamination of the surface shell

Figure 6

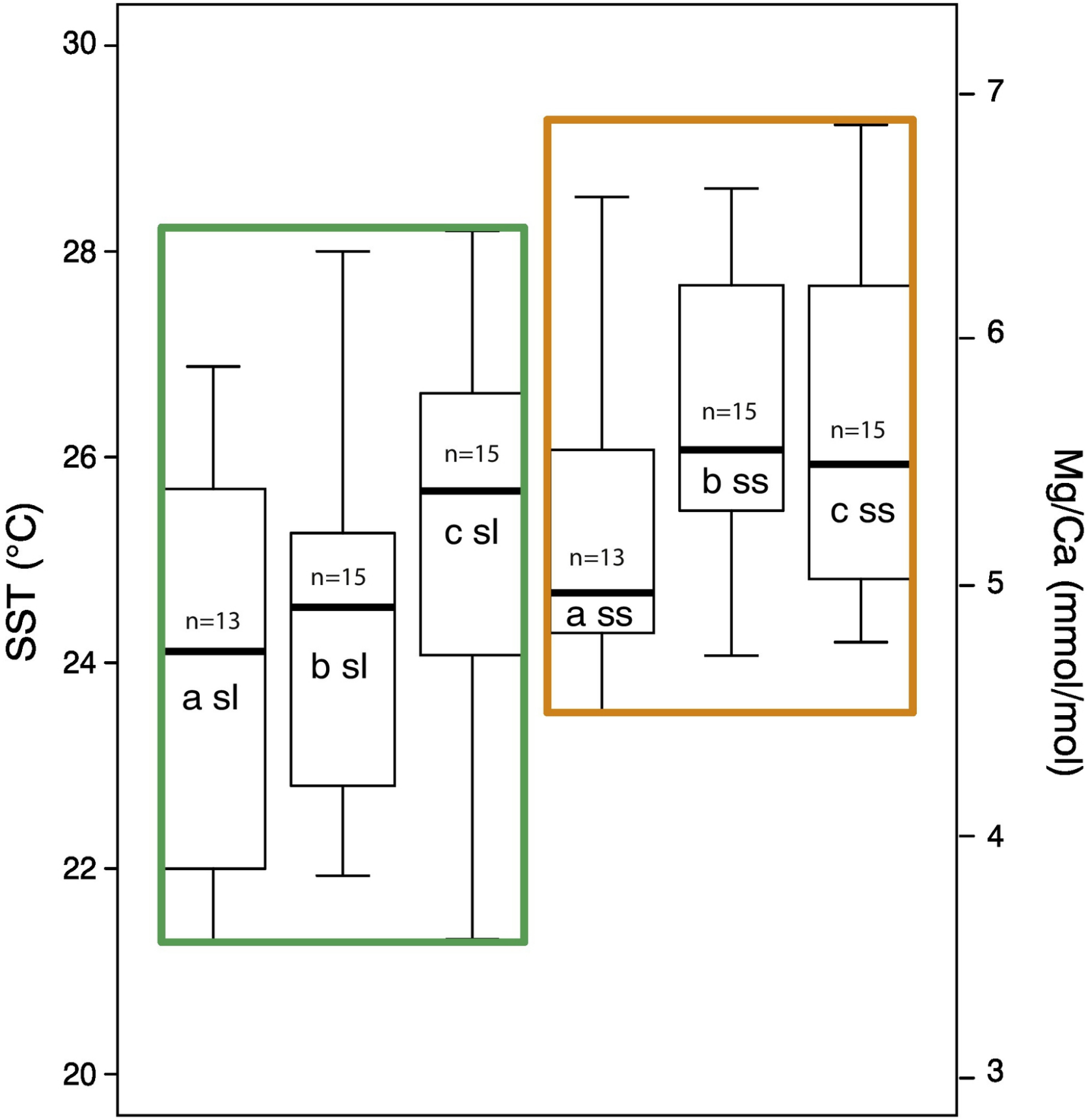
30
28
26
24
22
20
SST (°C)
7
6
5
4
3
Mg/Ca (mmol/mol)
n=13
a sl
n=15
b sl
n=15
c sl
n=13
a ss
n=15
b ss
n=15
c ss

Figure 7

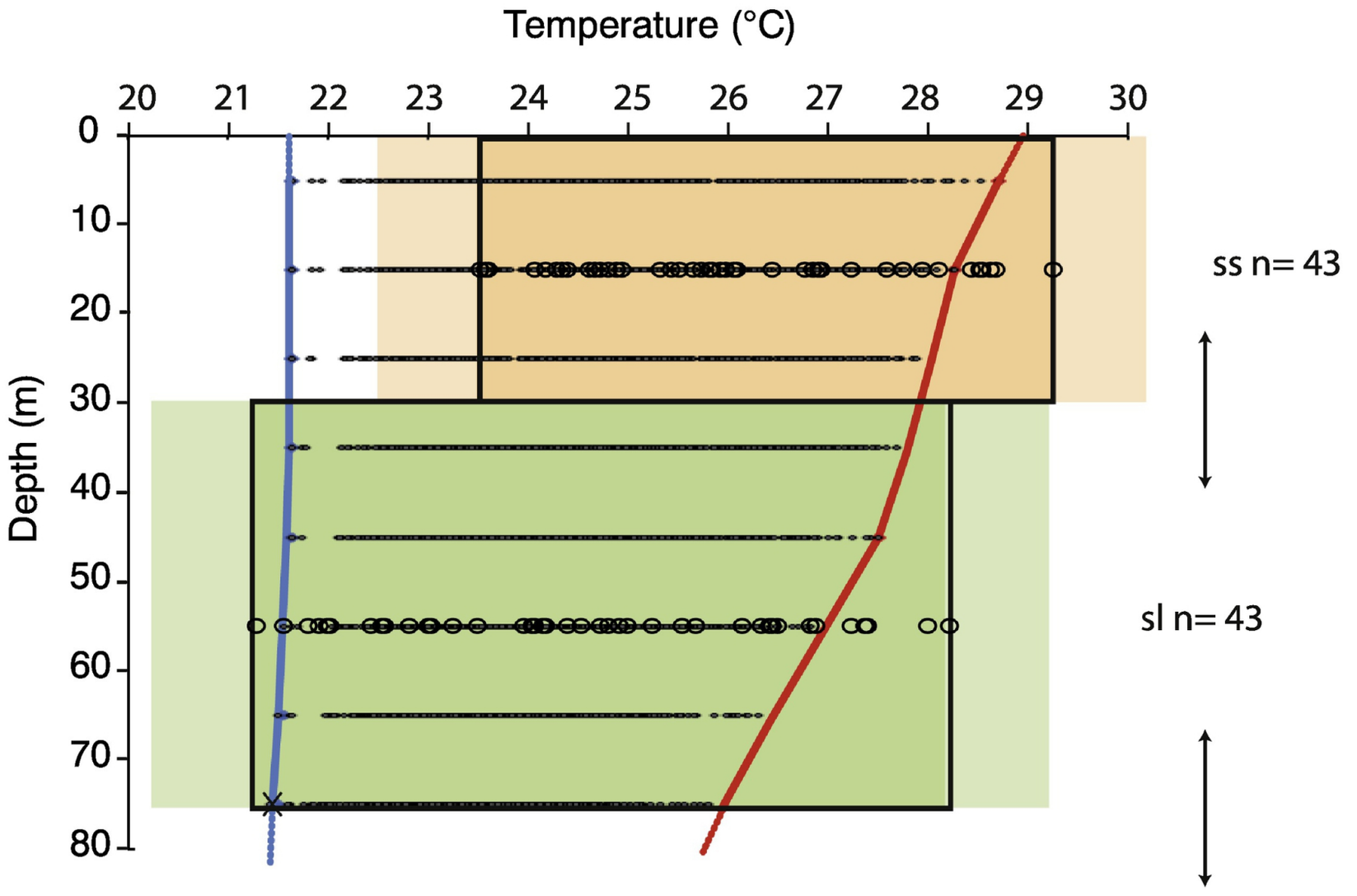

WOA05 data SST

- colder months recorded on last 37 years
- warmer months recorded on last 37 years
- uncertainty about the depth of life of morphotypes
- mean monthy temperatures on last 37 years

Temperature from Mg/Ca by LA-ICPMS in Holocene

- area of *G.ruber* ss temperature range
- potential ss error of temperature range
- area of *G.ruber* sl temperature range
- potential sl error of temperature range
- *G.ruber* ss and sl values on individual foraminifera

Figure 8

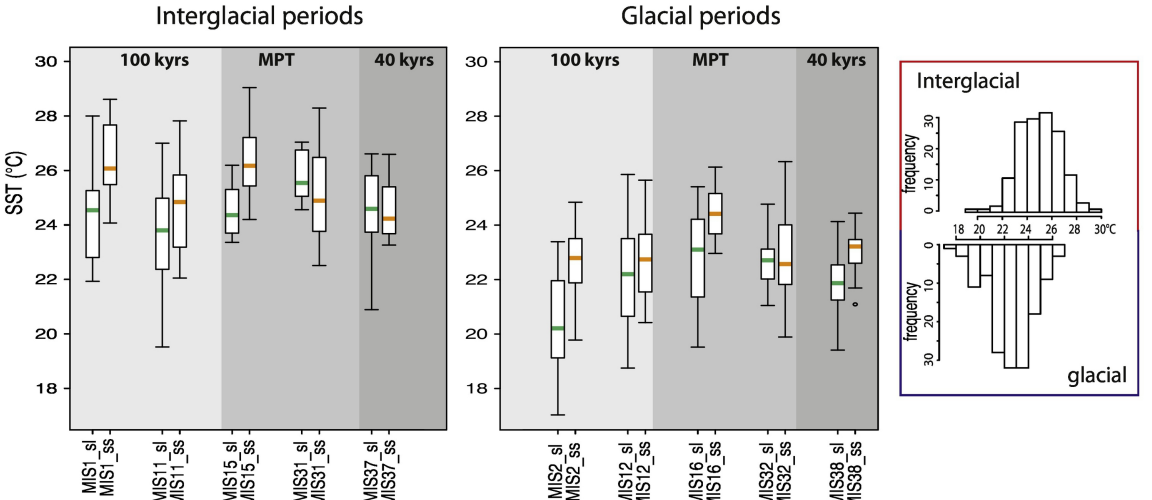
Interglacial periods
Glacial periods
100 kyrs
MPT
40 kyrs
SST (°C)
30
28
26
24
22
20
18
MIS1_sl
MIS1_ss
MIS11_sl
MIS11_ss
MIS15_sl
MIS15_ss
MIS31_sl
MIS31_ss
MIS37_sl
MIS37_ss
MIS2_sl
MIS2_ss
MIS12_sl
MIS12_ss
MIS16_sl
MIS16_ss
MIS32_sl
MIS32_ss
MIS38_sl
MIS38_ss
Interglacial
frequency
0
10
20
30
18
20
22
24
26
28
30°C
glacial

Figure 9

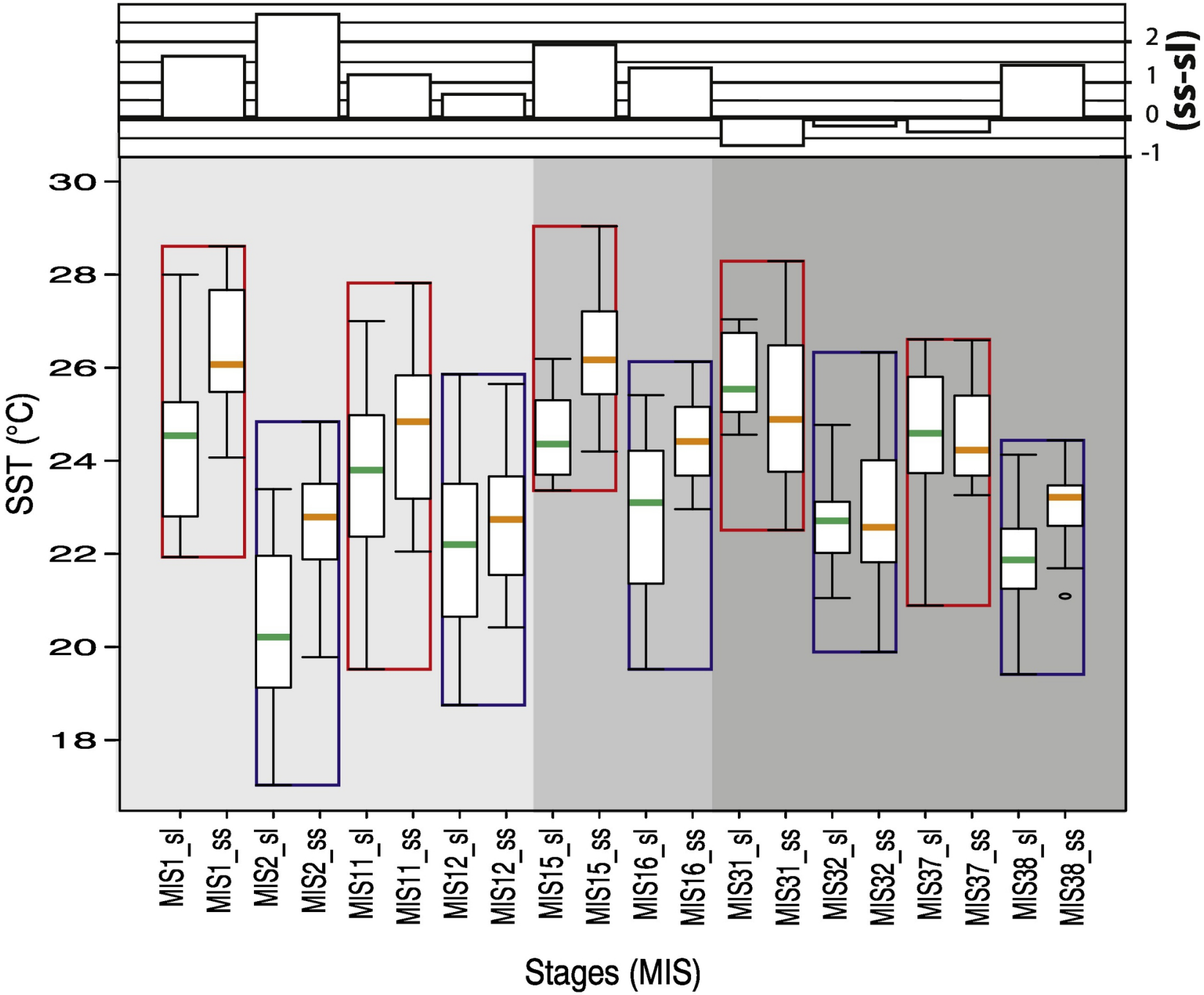
(ss-sl)
2
1
0
-1
SST (°C)
30
28
26
24
22
20
18
MIS1_sl
MIS1_ss
MIS2_sl
MIS2_ss
MIS11_sl
MIS11_ss
MIS12_sl
MIS12_ss
MIS15_sl
MIS15_ss
MIS16_sl
MIS16_ss
MIS31_sl
MIS31_ss
MIS32_sl
MIS32_ss
MIS37_sl
MIS37_ss
MIS38_sl
MIS38_ss
Stages (MIS)

Figure 10